

2D+3D facial expression recognition via embedded tensor manifold regularization

Yunfang Fu* Qiuqi Ruan[†] Ziyang Luo[‡] Gaoyun An[§] Yi Jin[¶] Jun Wan^{||}

February 1, 2022

Abstract

In this paper, a novel approach via embedded tensor manifold regularization for 2D+3D facial expression recognition (FERETMR) is proposed. Firstly, 3D tensors are constructed from 2D face images and 3D face shape models to keep the structural information and correlations. To maintain the local structure (geometric information) of 3D tensor samples in the low-dimensional tensors space during the dimensionality reduction, the ℓ_0 -norm of the core tensors and a tensor manifold regularization scheme embedded on core tensors are adopted via a low-rank truncated Tucker decomposition on the generated tensors. As a result, the obtained factor matrices will be used for facial expression classification prediction. To make the resulting tensor optimization more tractable, ℓ_1 -norm surrogate is employed to relax ℓ_0 -norm and hence the resulting tensor optimization problem has a nonsmooth objective function due to the ℓ_1 -norm and orthogonal constraints from the orthogonal Tucker decomposition. To efficiently tackle this tensor optimization problem, we establish the first-order optimality condition in terms of stationary points, and then design a block coordinate descent (BCD) algorithm with convergence analysis and the computational complexity. Numerical results on BU-3DFE database and Bosphorus databases demonstrate the effectiveness of our proposed approach.

Key words. 2D+3D facial expression recognition, tensor manifold regularization, Orthogonal Tucker decomposition, tensor optimization, BCD algorithm

*School of Computer Science and Engineering, Shijiazhuang University, Shijiazhuang 050035, China, Institute of Information Science, Beijing Jiaotong University, Beijing 100044, China, and Beijing Key Laboratory of Advanced Information Science and Network Technology, Beijing 100044, China. e-mail: fu_yunfang@126.com.

[†]Institute of Information Science, Beijing Jiaotong University, Beijing 100044, China, and Beijing Key Laboratory of Advanced Information Science and Network Technology, Beijing 100044, China. e-mail: qqruan@bjtu.edu.cn.

[‡]Corresponding author, Department of Mathematics, Beijing Jiaotong University, Beijing 100044, China. (zyluo@bjtu.edu.cn).

[§]Institute of Information Science, Beijing Jiaotong University, Beijing 100044, China, and Beijing Key Laboratory of Advanced Information Science and Network Technology, Beijing 100044, China. e-mail: gyan@bjtu.edu.cn.

[¶]Institute of Information Science, Beijing Jiaotong University, Beijing 100044, China, and Beijing Key Laboratory of Advanced Information Science and Network Technology, Beijing 100044, China. e-mail: yjin@bjtu.edu.cn.

^{||}National Laboratory of Pattern Recognition, Institute of Automation, Chinese Academy of Sciences, Beijing 100190, China. e-mail: jun.wan@nlpr.ia.ac.cn.

1 Introduction

Facial expressions, as a way of no-verbal communication and a tool of delivering social information among human beings, are utilized to measure, interpretate and compute the human emotion. Hence, automatic recognition of facial expressions has attracted a great deal of interest, with wide applications in various domains such as psychology, human-machine interaction, transport security, health monitoring, computer graphics, pattern recognition, *etc.* And it plays a crucial role in affective computing, computer vision and multimedia research [7].

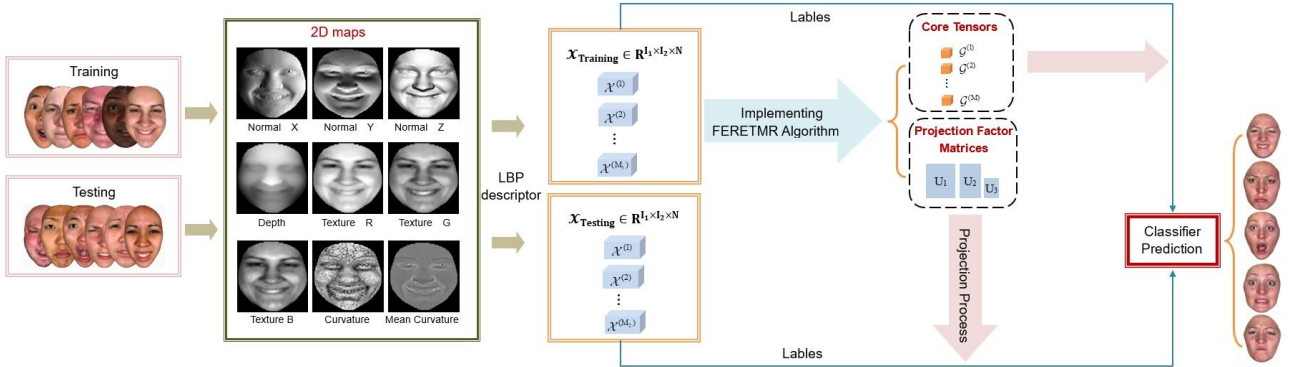


Figure 1: A flowchart of the proposed approach (FERETMR) on BU-3DFE database.

In the last several decades, the majority of research for FER focused on 2D face images [40, 51] or video sequences [8, 56] in terms of feature extraction based on facial expression, face detection and classification. With the evolution of the algorithm in some close fields, such as face marking, feature engineering, its performance has been greatly improved. However, 2D approaches based on the facial texture analysis have disadvantages suffering from illumination and pose variations, and possible occlusions [30].

With the fast development of 3D acquisition equipments, 3D FER by utilizing 3D face scans has gained a great deal of attention due to more robustness to illumination and pose variations. Moreover, 3D face scans represented by 3D point sets have the ability to capture accurately the muscle movements of the facial skin surface, which are beneficial for FER.

The key of 3D facial expression recognition and analysis lies mainly on data description, feature extraction, and effective dimensionality reduction methods. As the very start in 3D FER, the data description is the most fundamental and crucial. A simple but widely used way of the data description in the literature on 3D FER is the *vectorization* (See, e.g., [24, 25, 31, 37, 38, 45, 46, 49, 55, 56]). However, the main drawback that vectorization suffers is the loss of the internal structure information of the data samples in which potential or inherent sparsity may hidden, and hence the dimensionality curse comes along by dismissing these favorable structural properties. To alleviate this issue, a more natural way to describe 3D facial expression data is using tensors, which not only maintains the spacial structure but also admits sparse representation when appropriate tensor decomposition is chosen, by employing tools from tensor analysis. At present, the existing methods using tensors to describe 3D facial expression data are mostly based on tensor decomposition [13–17, 20, 21], which have opened up a new

technology direction and made some progress. However, the local structure (geometric information) of 3D tensor samples in these methods are not maintained in the low-dimensional tensors space during the dimensionality reduction.

To solve the above problem, a novel approach for 2D+3D FER via embedded tensor manifold regularization is proposed in this paper, with detailed flowchart shown in Fig. 1. At first, a novel data representation is given, i.e., 3D tensors are constructed by stacking nine different features extracted from textured 3D scans to keep the structural information and correlations between multi-modal data (2D face images and 3D face shape models). Tensor decomposition based on low-rank approximation is regarded as a powerful technique to be able to extract useful and discriminative low-dimensional information from the high-dimensional data. And Tucker decomposition is one of the widely utilized forms of low-rank tensor decomposition, which decomposes a tensor into a product of a number of factor matrices and a core tensor. We focus on Tucker decomposition in this paper. Based on orthogonal Tucker decomposition of the generated 3D tensors, our goal in this paper is to find projection factor matrices and a set of core tensors of relatively small sizes for the facial expression classification prediction. Since potential similarities may inherit in the tensor modelling process, the resulting 3D tensors, probably of high dimension for real data sets, can be embedded into low-dimensional spaces. A tensor reduction dimensionality technique is then utilized to the core tensors generated from orthogonal Tucker decomposition, equipped with an embedded tensor manifold regularization scheme to preserve the geometrical information during the dimension reduction. Meanwhile, the ℓ_1 -regularization term is employed to promote sparsity structure on the involved core tensors. Finally, an efficient optimization algorithm with the block coordinate descent (BCD) framework is designed to solve the resulting tensor optimization problem. Thus, a novel tensor optimization model with an embedded tensor manifold regularization and sparsity based on the Tucker decomposition is then built to extract the useful and discriminative low-dimensional information from the generated 3D tensors model by using the tensor reduction dimensionality strategy. At the same time, Optimality analysis and stationarity are detailed according to the resulting optimization problem. The analysis of convergence and the computational complexity of the proposed algorithm is also shown, where the computational complexity scales linearly with respect to the size of the constructed tensors and the number of the tensor samples, respectively. To verify the effectiveness of our proposed approach, the multi-class-SVM is utilized for expression classification prediction.

The main contributions of our work are summarized below:

- A novel data representation is given, in which a 3D tensor model is constructed by utilizing both 2D and 3D face data. This kind of data representation overcomes the issues that the small sample size (SSS) problem and the dimensionality disaster due to vector representation.
- A tensor dimensionality reduction technique is utilized to the core tensors generated from orthogonal Tucker decomposition via an embedded tensor manifold regularization scheme to preserve the geometrical information during the dimensionality reduction.
- An efficient algorithm with the block coordinate descent (BCD) framework is designed to effectively solve the proposed tensor optimization model, and is applied into 2D+3D FER.

- Optimality analysis and stationarity are detailed according to the resulting optimization problem. Meanwhile the convergence and computational complexity of the proposed approach are effectively analyzed.

The rest of the paper is organized as follows. Related works are recalled including preliminaries on tensors in Section II. The details of our proposed optimization model are described in Section III. Experiment results and analysis are reported in Section IV, and conclusions are drawn in Section V.

2 Related Works

2.1 Tensor Basics

Throughout the paper, vectors will be written by lowercase letters, e.g., x , matrices by capital letters, e.g., X , and tensors by calligraphic letters, e.g., \mathcal{X} . The symbols \otimes , \circ and $*$ are used to denote the Kronecker, outer and Hadamard product, respectively.

Given an N th-order tensor $\mathcal{X} = (\mathcal{X}_{i_1 \dots i_N}) \in \mathbb{R}^{I_1 \times I_2 \times \dots \times I_N}$, its mode- n unfolding, denoted by $X_{(n)}$, is a matrix of size $I_n \times \prod_{k \neq n, k=1}^N I_k$, with entries

$$(X_{(n)})_{ij} = \mathcal{X}_{i_1 \dots i_N}, i = i_n, j = 1 + \sum_{k=1, k \neq n}^N (i_k - 1) \prod_{m=1, m \neq n}^k I_m.$$

The mode- n product of \mathcal{X} with a matrix $U \in \mathbb{R}^{I_n \times R_n}$, termed as $\mathcal{X} \times_n U$, is a tensor $\mathcal{Y} \in \mathbb{R}^{I_1 \times I_2 \times \dots \times R_n \times \dots \times I_N}$ with its entries

$$\mathcal{Y}_{i_1 i_2 \dots r_n \dots i_N} = \sum_{i_n=1}^{I_n} \mathcal{X}_{i_1 i_2 \dots i_n \dots i_N} U_{r_n i_n}.$$

Given any two tensors $\mathcal{X}, \mathcal{Y} \in \mathbb{R}^{I_1 \times I_2 \times \dots \times I_N}$, the inner product $\langle \mathcal{X}, \mathcal{Y} \rangle$ is defined as the sum of all the products of their corresponding entries, that is,

$$\langle \mathcal{X}, \mathcal{Y} \rangle = \sum_{i_1=1}^{I_1} \dots \sum_{i_N=1}^{I_N} \mathcal{X}_{i_1 \dots i_N} \mathcal{Y}_{i_1 \dots i_N}.$$

The tensor Frobenius norm, induced by the above inner product, is defined by

$$\|\mathcal{X}\|_F := \sqrt{\langle \mathcal{X}, \mathcal{X} \rangle}.$$

For sparsity characterization, the so-called ℓ_0 -norm (quasi-norm mathematically) of vectors can be naturally extended to high-order tensors, denoted by $\|\mathcal{X}\|_0$, which counts the number of nonzero entries in \mathcal{X} , i.e.,

$$\|\mathcal{X}\|_0 := \#\{(i_1, i_2, \dots, i_N) : \mathcal{X}_{i_1 \dots i_N} \neq 0\}.$$

Analogous to vectors, the tensor ℓ_1 -norm $\|\mathcal{X}\|_1$ also serves as the tightest convex surrogate of $\|\mathcal{X}\|_0$ and is defined by

$$\|\mathcal{X}\|_1 := \sum_{i_1=1}^{I_1} \sum_{i_2=1}^{I_2} \dots \sum_{i_N=1}^{I_N} |\mathcal{X}_{i_1 i_2 \dots i_N}|,$$

respectively.

2.2 Tensorial Data Reduction

2.2.1 Orthogonal Tucker Decomposition

Tucker decomposition, which decomposes a tensor into a core tensor multiplied by a set of factor matrices along each mode, is one of the most widely used tensor decomposition methods. Usually the orthogonality constraint is imposed to each factor matrix which yields the so-called orthogonal Tucker decomposition. Mathematically, for a given N th-order tensor $\mathcal{X} \in \mathbb{R}^{I_1 \times I_2 \times \dots \times I_N}$, its orthogonal Tucker decomposition can be written as

$$\mathcal{X} = \mathcal{G} \prod_{n=1}^N \times_n U_n, \quad \text{with } U_n \in \text{St}(I_n, R_n), n = 1, \dots, N,$$

where $\mathcal{G} \in \mathbb{R}^{R_1 \times R_2 \times \dots \times R_N}$ is the core tensor, $\text{St}(I_n, R_n) := \{U_n \in \mathbb{R}^{I_n \times R_n} | U_n^T U_n = \mathbf{I}_{R_n}\}$ is the so-called the Stiefel manifold [11], and U_n 's are factor matrices which are partially orthogonal. Here \mathbf{I}_{R_n} denotes the identity matrix of size $R_n \times R_n$.

2.2.2 Tensor Sparse Representation

Sparse representation (SR) method, which is stemmed from compressed sensing (CS) [10], is widely applied into extensive application fields, such as pattern recognition, signal processing, machine learning, image processing, computer vision [42, 44], etc. On the basis of the orthogonal Tucker decomposition, a structured sparse representation or approximation imposed on the core tensor can be obtained as follows

$$\min_{\{U_n\}, \mathcal{G}} \left\{ \|\mathcal{G}\|_0 : \mathcal{X} = \mathcal{G} \prod_{n=1}^N \times_n U_n, U_n \in \text{St}(I_n, R_n) \right\}. \quad (1)$$

Since the ℓ_0 -norm is non-convex and discontinuous, problem (1) is NP-hard generally and difficult to compute its exact optimal solutions. One of the most popular relaxation strategies is to use the ℓ_1 -norm [6, 43, 53] as a surrogate since the ℓ_1 -norm is shown to be the tightest convex relaxation within the unit ball. The resulting continuous optimization problem takes the form of

$$\min_{\{U_n\}, \mathcal{G}} \left\{ \|\mathcal{G}\|_1 : \mathcal{X} = \mathcal{G} \prod_{n=1}^N \times_n U_n, U_n \in \text{St}(I_n, R_n) \right\}. \quad (2)$$

2.2.3 Manifold Regularization Extension

Inspired by the work [1, 26, 57] based on manifold learning, the manifold regularization framework is utilized to efficiently build a nearest neighborhood graph information for preserving the local geometry structure of higher order tensor data. The main idea is: given M tensors of the same size $I_1 \times I_2 \times \dots \times I_N$, say $\mathcal{X}^{(1)}, \mathcal{X}^{(2)}, \dots, \mathcal{X}^{(M)}$, find partially orthogonal matrices U_1, \dots, U_N to decompose these M tensors simultaneously in the Tucker sense, i.e.,

$$\mathcal{X}^{(i)} = \mathcal{G}^{(i)} \times_1 U_1 \times_2 \dots \times_N U_N, \quad i \in [M], \quad (3)$$

where $\mathcal{G}^{(i)} \in \mathbb{R}^{R_1 \times \dots \times R_N}$, $i = 1, \dots, M$ are of reduced dimensions, comparing to the original $\mathcal{X}^{(i)}$'s. Concisely, by stacking all $\mathcal{X}^{(i)}$'s and $\mathcal{G}^{(i)}$'s into $(N+1)$ th-order tensors, namely $\mathcal{X} \in \mathbb{R}^{I_1 \times \dots \times I_N \times M}$ and

$\mathcal{G} \in \mathbb{R}^{R_1 \times \dots \times R_N \times M}$, the above data reduction via decomposition can be written as

$$\mathcal{X} = \mathcal{G} \times_1 U_1 \times_2 \dots \times_N U_N. \quad (4)$$

This is indeed an orthogonal Tucker decomposition for \mathcal{X} with \mathbf{I}_M as the last mode factor matrix. To preserve the potential or prior local similarity among these M original tensors $\mathcal{X}^{(i)}$'s, one would expect to reflect such similarities among the resulting low-dimensional tensors $\mathcal{G}^{(i)}$'s. Adopt the following weight matrix $W \in \mathbb{R}^{M \times M}$ with entries

$$w_{ij} = \begin{cases} 1, & \text{if } \mathcal{X}^{(i)} \in \mathcal{N}_k(\mathcal{X}^{(j)}) \text{ or } \mathcal{X}^{(j)} \in \mathcal{N}_k(\mathcal{X}^{(i)}) \\ 0, & \text{otherwise.} \end{cases}$$

where $\mathcal{N}_k(\cdot)$ is the set consisting of k -nearest neighbors of the object. To keep local similarity among low-dimensional projections $\mathcal{G}^{(i)}$'s, it is then reasonable to construct the following Stiefel manifold constrained tensor optimization model

$$\min_{U_n \in \text{St}(I_n, R_n)} \sum_{i \neq j, i, j=1}^M \left\| \mathcal{G}^{(i)} - \mathcal{G}^{(j)} \right\|_F^2 w_{ij}. \quad (5)$$

3 The Proposed Approach

3.1 The Manifold Regularization Orthogonal Tucker Decomposition Model

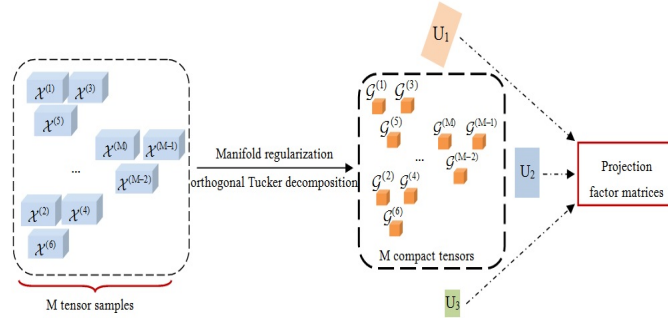


Figure 2: Idea description of our proposed approach.

Let $\mathcal{X}^{(1)}, \dots, \mathcal{X}^{(M)} \in \mathbb{R}^{I_1 \times I_2 \times N}$ be M samples of generated 3D face data by naturally storing N features with image size $I_1 \times I_2$. Stacking all these samples into a 4th-order tensor, denoted as $\mathcal{X} \in \mathbb{R}^{I_1 \times I_2 \times N \times M}$. Adopting the idea of sparse tensor representation, along with the low-rank Tucker decomposition with embedded tensor manifold regularization, as described in Subsection 2.2, we construct the following sparse tensor optimization for tensor data reduction

$$\begin{aligned} \min \quad & \mathcal{L} \left(\{\mathcal{G}^{(i)}\}_{i=1}^M, \{U_n\}_{n=1}^3 \right) \\ \text{s.t.} \quad & \mathcal{G}^{(i)} \in \mathbb{R}^{R_1 \times R_2 \times N}, \quad i = 1, \dots, M, \\ & U_n \in \text{St}(I_n, R_n), \quad n = 1, 2, 3. \end{aligned} \quad (6)$$

Here the objective function is

$$\begin{aligned}
& \mathfrak{L} \left(\{\mathcal{G}^{(i)}\}_{i=1}^M, \{U_n\}_{n=1}^3 \right) \\
&= \frac{1}{\gamma} \sum_{i=1}^M \left\| \mathcal{G}^{(i)} \right\|_1 + \frac{1}{2} \sum_{i=1}^M \left\| \mathcal{X}^{(i)} - \mathcal{G}^{(i)} \prod_{n=1}^3 \times_n U_n \right\|_F^2 \\
&+ \frac{1}{\beta} \sum_{i \neq j, i, j \in [M]} \left\| \mathcal{G}^{(i)} - \mathcal{G}^{(j)} \right\|_F^2 w_{ij}
\end{aligned} \tag{7}$$

with the tradeoff parameters $\gamma, \beta > 0$ for controlling the three terms corresponding to the sparsity of core tensors, the reconstruction error, and the tensor geometry information preservation, respectively, and $I_3 = R_3 = N$.

3.2 Optimality Analysis and Stationarity

Before the algorithm design for solving problem (6), we address the optimality analysis in terms of stationary points for theoretical preparation. Recall from [33, Definition 8.3] that the subdifferential of a proper closed function f at a given point x in its domain $\text{dom} f$, usually termed as $\partial f(x)$ is defined as

$$\partial f(x) := \{v : \exists x^k \rightarrow x \text{ and } v^k \in \hat{\partial} f(x^k), v^k \rightarrow v\}.$$

where

$$\hat{\partial} f(x^k) = \left\{ v^k : \lim_{y \rightarrow x^k, y \neq x^k} \frac{f(y) - f(x^k) - \langle v^k, y - x^k \rangle}{\|y - x^k\|} \geq 0 \right\}.$$

If f is differentiable at x , then the subdifferential $\partial f(x)$ reduces to the gradient $\nabla f(x)$.

Definition 1. We call $\mathcal{H}^* := (\{(\mathcal{G}^{(i)})^*\}_{i=1}^M, \{U_n^*\}_{n=1}^3)$ a stationary point of problem (6) if $\mathcal{O} \in \partial F(\mathcal{H}^*)$, or equivalently,

$$\begin{cases} \mathcal{O} \in \partial_{\mathcal{G}^{(i)}} \mathfrak{L}(\mathcal{H}^*), & i = 1, \dots, M, \\ \mathcal{O} \in \nabla_{U_n} \mathfrak{L}(\mathcal{H}^*) + N_{St(I_n, R_n)}(U_n^*), & n = 1, 2, 3, \end{cases} \tag{8}$$

where $N_{St(I_n, R_n)}(U_n^*)$ is the normal space to $St(I_n, R_n)$ at U_n , taking the form of

$$N_{St(I_n, R_n)}(U_n^*) = \{U_n^* S : S \in \mathbb{R}^{R_n \times R_n}, S^T = S\}.$$

The following theorem states the first-order optimality condition of problem (6) in terms of the stationarity defined as above.

Theorem 3.1. For problem (6), if $\mathcal{H}^* = (\{(\mathcal{G}^{(i)})^*\}_{i=1}^M, \{U_n^*\}_{n=1}^3)$ is a local minimizer, then \mathcal{H}^* is a stationary point, i.e., (8) holds at \mathcal{H}^* .

3.3 Solving the Optimization Model

We will adopt the block coordinate descent (BCD) scheme in the algorithm design for solving the proposed tensor optimization problem (6). By introducing the indicator function $\delta_{St(I_n, R_n)}$ defined as

$$\delta_{St(I_n, R_n)}(U) = \begin{cases} 0, & \text{if } U \in St(I_n, R_n); \\ +\infty, & \text{otherwise.} \end{cases} \tag{9}$$

we can rewrite (6) into the following nonsmooth tensor optimization problem

$$\min_{\{\mathcal{G}^{(i)}\}_{i=1}^M, \{U_n\}_{n=1}^3} \mathfrak{L} \left(\{\mathcal{G}^{(i)}\}_{i=1}^M, \{U_n\}_{n=1}^3 \right) + \sum_{n=1}^3 \delta_{\text{St}(I_n, R_n)}(U_n) \quad (10)$$

Denote $F(\{\mathcal{G}^{(i)}\}_{i=1}^M, \{U_n\}_{n=1}^3)$ as the objective function in (10). One can see that the involved nonsmooth terms in F are separable in $\mathcal{G}^{(i)}$'s and U_n 's. This observation inspires us to employ the block coordinate descent (BCD) method ([39]) with the following updates in the Gauss-Siedel fashion:

$$\left\{ \begin{array}{l} U_1^{[k+1]} = \arg \min_{U_1} F \left(\{\mathcal{G}_k^{(i)}\}_{i=1}^M, U_1, U_2^{[k]}, U_3^{[k]} \right), \\ U_2^{[k+1]} = \arg \min_{U_2} F \left(\{\mathcal{G}_k^{(i)}\}_{i=1}^M, U_1^{[k+1]}, U_2, U_3^{[k]} \right), \\ U_3^{[k+1]} = \arg \min_{U_3} F \left(\{\mathcal{G}_k^{(i)}\}_{i=1}^M, U_1^{[k+1]}, U_2^{[k+1]}, U_3 \right), \\ \mathcal{G}_{k+1}^{(1)} = \arg \min_{\mathcal{G}^{(1)}} F \left(\mathcal{G}^{(1)}, \mathcal{G}_k^{(2)}, \dots, \mathcal{G}_k^{(M)}, \{U_n^{[k+1]}\}_{n=1}^3 \right), \\ \mathcal{G}_{k+1}^{(2)} = \arg \min_{\mathcal{G}^{(2)}} F \left(\mathcal{G}_{k+1}^{(1)}, \mathcal{G}^{(2)}, \mathcal{G}_k^{(3)}, \dots, \mathcal{G}_k^{(M)}, \{U_n^{[k+1]}\}_{n=1}^3 \right), \\ \vdots \\ \mathcal{G}_{k+1}^{(M)} = \arg \min_{\mathcal{G}^{(M)}} F \left(\mathcal{G}_{k+1}^{(1)}, \dots, \mathcal{G}_{k+1}^{(M-1)}, \mathcal{G}^{(3)}, \{U_n^{[k+1]}\}_{n=1}^3 \right), \end{array} \right. \quad (11)$$

For simplicity, we will remove the iterate number k and $k+1$ from all decision variables $\mathcal{G}^{(i)}$'s and U_n 's, and use $\hat{\mathcal{G}}^{(i)}$'s and \hat{U}_n 's for the new updates in the remainder of this subsection.

The subproblems for updating U_n 's take the form of

$$\begin{aligned} \hat{U}_n &= \arg \min_{U_n} \frac{1}{2} \sum_{i=1}^M \left\| X_{(n)}^{(i)} - U_n \Phi_{(n)}^i \right\|_F^2 + \delta_{\text{St}(I_n, R_n)}(U_n) \\ &= \arg \max_{U_n} \left\langle U_n, \sum_{i=1}^M X_{(n)}^{(i)} \Phi_{(n)}^i{}^T \right\rangle - \delta_{\text{St}(I_n, R_n)}(U_n) \\ &= Y_n Z_n^T =: \text{qf} \left(\sum_{i=1}^M X_{(n)}^{(i)} \Phi_{(n)}^i{}^T \right), \end{aligned} \quad (12)$$

where $\Phi_n^{(i)} = (\mathcal{G}^{(i)} \prod_{k=1, k \neq n}^3 \times_k U_k)_{(n)}$, $Y_n \in \text{St}(I_n, R_n)$ and $Z_n \in \text{St}(R_n, R_n)$ are the matrices consisting of the left- and right- singular vectors of the matrix argument, and $\text{qf}(\cdot)$ stands for the product matrix $Y_n Z_n^T$. Here the last equality is due to the *von Neumann's trace inequality* in [28].

The subproblems for updating $\mathcal{G}^{(i)}$'s take the form of

$$\begin{aligned}
\hat{\mathcal{G}}^{(i)} &= \arg \min_{\mathcal{G}^{(i)}} \frac{1}{\gamma} \left\| \mathcal{G}^{(i)} \right\|_1 + \frac{1}{2} \left\| \mathcal{X}^{(i)} - \mathcal{G}^{(i)} \prod_{n=1}^4 \times_n U_n \right\|_F^2 \\
&\quad + \frac{1}{\beta} \sum_{j \neq i} \left\| \mathcal{G}^{(i)} - \mathcal{G}^{(j)} \right\|_F^2 w_{ij} \\
&= \arg \min_{\mathcal{G}^{(i)}} \frac{1}{\gamma} \left\| \mathcal{G}^{(i)} \right\|_1 + \frac{1}{2} \left\| \mathcal{X}^{(i)} \prod_{n=1}^3 \times_n U_n^T - \mathcal{G}^{(i)} \right\|_F^2 \\
&\quad + \frac{1}{\beta} \sum_{j \neq i} \left\| \mathcal{G}^{(i)} - \mathcal{G}^{(j)} \right\|_F^2 w_{ij} \\
&= \left(\arg \min_{\mathcal{G}_{i_1 i_2 i_3}^{(i)}} \frac{1}{\gamma} \left| \mathcal{G}_{i_1 i_2 i_3}^{(i)} \right| + \frac{1}{2} \left(\mathcal{G}_{i_1 i_2 i_3}^{(i)} - \mathcal{D}_{i_1 i_2 i_3}^{(i)} \right)^2 \right. \\
&\quad \left. + \sum_{j \neq i} \frac{w_{ij}}{\beta} \left(\mathcal{G}_{i_1 i_2 i_3}^{(i)} - \mathcal{G}_{i_1 i_2 i_3}^{(j)} \right)^2 \right)_{i_1=1, i_2=1, i_3=1}^{R_1, R_2, R_3} \\
&= \left(\arg \min_{\mathcal{G}_{i_1 i_2 i_3}^{(i)}} \tau^{(i)} \left| \mathcal{G}_{i_1 i_2 i_3}^{(i)} \right| \right. \\
&\quad \left. + \frac{1}{2} \left(\mathcal{G}_{i_1 i_2 i_3}^{(i)} - \alpha_{i_1 i_2 i_3}^{(i)} \right)^2 \right)_{i_1=1, i_2=1, i_3=1}^{R_1, R_2, R_3} \\
&= \left(\text{Prox}_{\tau^{(i)}|\cdot|}(\alpha_{i_1 i_2 i_3}^{(i)}) \right)_{i_1=1, i_2=1, i_3=1}^{R_1, R_2, R_3},
\end{aligned} \tag{13}$$

where $\mathcal{D}^{(i)} = \mathcal{X}^{(i)} \prod_{n=1}^3 \times_n U_n^T$, $\tau^{(i)} = \frac{\beta}{\gamma(\beta+2 \sum_{j \neq i} w_{ij})}$, $\alpha_{i_1 i_2 i_3}^{(i)} = \frac{\beta \mathcal{D}_{i_1 i_2 i_3}^{(i)} + \sum_{j \neq i} w_{ij} \mathcal{G}_{i_1 i_2 i_3}^{(j)}}{\beta+2 \sum_{j \neq i} w_{ij}}$, and $\text{Prox}_{\tau^{(i)}|\cdot|}(\cdot)$ is the proximal mapping (See, e.g., [33]) associated with the function $f(t) = \tau^{(i)}|t|$, defined as

$$\text{Prox}_f(x) = \arg \min_t \left\{ f(t) + \frac{1}{2}(t-x)^2 \right\}. \tag{14}$$

It is worth mentioning that the involved function $\text{Prox}_{\tau^{(i)}|\cdot|}(\cdot)$ for updating $\mathcal{G}^{(i)}$ has the following explicit formula

$$\left(\text{Prox}_{\tau^{(i)}|\cdot|}(\alpha_{i_1 i_2 i_3}^{(i)}) \right)_{i_1=1, i_2=1, i_3=1}^{R_1, R_2, R_3} = \left(\max\{|\alpha_{i_1 i_2 i_3}^{(i)}| - \tau^{(i)}, 0\} \text{sign}(\alpha_{i_1 i_2 i_3}^{(i)}) \right)_{i_1=1, i_2=1, i_3=1}^{R_1, R_2, R_3} \tag{15}$$

which is actually the tensor version of the so-called soft-thresholding operator (See, e.g., [3]). For simplicity, we write the involved *tensor soft-thresholding operator* as $\text{Prox}_{\tau^{(i)}\|\cdot\|_1}(\cdot)$. Thus, (13) can be written as

$$\hat{\mathcal{G}}^{(i)} = \text{Prox}_{\tau^{(i)}\|\cdot\|_1} \left(\frac{\beta \mathcal{X}^{(i)} \prod_{n=1}^3 \times_n U_n^T + \sum_{j \neq i} w_{ij} \mathcal{G}^{(j)}}{\beta + 2 \sum_{j \neq i} w_{ij}} \right). \tag{16}$$

Such an operator is continuous, as illustrated via the graph of the univariate case shown in Fig. 3.

The corresponding algorithmic framework is then presented in Algorithm 1.

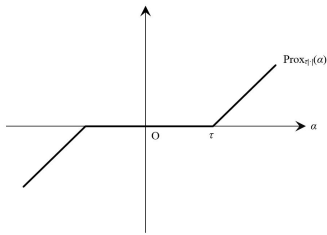


Figure 3: The graph of $\text{Prox}_{\tau|\cdot|}(\alpha)$.

Algorithm 1 Solving Problem (10) by BCD

Require: M sample tensors $\{\mathcal{X}^{(i)}\}_{i=1}^M \in \mathbb{R}^{I_1 \times I_2 \times I_3}$; Parameters γ, β ;

Ensure: Factor matrices $\{U_n\}_{n=1}^3$;

Step 0 Randomly initialize $\{\mathcal{G}^{(i)}\}_{i=1}^M, \{U_n\}_{n=1}^3$;

Step 1 Update U_n 's and $\mathcal{G}^{(i)}$'s by (11) with closed form solutions stated in (12) and (16);

Step 2 If some stopping criterion is satisfied then stop, otherwise go to Step 1.

3.4 Computational Complexity and Convergence

3.4.1 Computational Complexity Analysis

For each iteration, the computation cost for all U_n 's in (12) is of the order

$$O(R_1 R_2 R_3 (I_1 + I_2 + I_3)) + O(M I_1 I_2 I_3 (R_1 + R_2 + R_3)) + O(R_1^2 I_1 + R_2^2 I_2 + R_3^2 I_3),$$

where the first term comes from the computation for all $\Phi_{(n)}^{(i)}$'s, the second term from $\sum_{i=1}^M X_{(n)}^{(i)} \Phi_{(n)}^{(i)T}$, and the last term from the SVD.

According to the closed-form solution in (16), we can get the computation cost for updating all $\mathcal{G}^{(i)}$'s in each iteration of the order

$$O(M I_1 I_2 I_3 (R_1 + R_2 + R_3)) + O(k M R_1 R_2 R_3),$$

where the first term is the cost from the computation for all $\mathcal{D}^{(i)}$'s, and the second term for all involved $\tau^{(i)}$'s and all $\alpha_{i_1, i_2, i_3}^{(i)}$'s, in which k represents the number of nearest neighbors employed in the manifold construction.

Thus, the total cost in each iteration in Algorithm 1 is of the order

$$O(R_1 R_2 R_3 (I_1 + I_2 + I_3 + kM)) + O(M I_1 I_2 I_3 (R_1 + R_2 + R_3)) + O(R_1^2 I_1 + R_2^2 I_2 + R_3^2 I_3).$$

As one can see, for each iteration, Algorithm 1 scales linearly with respect to the number of tensor objects M , and also scales almost linearly with respect to the size of tensor objects $I_1 I_2 I_3$.

3.4.2 Convergence Analysis

As shown in Algorithm 1, the BCD scheme admits the non-increasing of the objective function \mathcal{L} of our proposed tensor optimization problem (6), and the lower bound for increment from the current iterate to the next is estimated in the following theorem.

Theorem 3.2. Let $\left\{ \left(\{\mathcal{G}_k^{(i)}\}_{i=1}^M, \{U_n^{[k]}\}_{n=1}^3 \right) \right\}$ be the sequence generated by Algorithm 1. Then the sequence of the objective values in problem (6) is non-increasing, and for any given integer $k \geq 0$, we have

$$\mathfrak{L} \left(\{\mathcal{G}_k^{(i)}\}_{i=1}^M, \{U_n^{[k]}\}_{n=1}^3 \right) - \mathfrak{L} \left(\{\mathcal{G}_{k+1}^{(i)}\}_{i=1}^M, \{U_n^{[k+1]}\}_{n=1}^3 \right) \geq \sum_{i=1}^M \left(\frac{1}{2} + \sum_{j \neq i} \frac{w_{ij}}{\beta} \right) \|\mathcal{G}_k^{(i)} - \mathcal{G}_{k+1}^{(i)}\|_F^2. \quad (17)$$

The bound of the decrease of objective function values as stated in (17) also indicates the stability of $\{\mathcal{G}_k^{(i)}\}$'s as k grows. More specifically, we have

$$\lim_{k \rightarrow \infty} \|\mathcal{G}_{k+1}^{(i)} - \mathcal{G}_k^{(i)}\|_F = 0, \quad \forall i = 1, \dots, M,$$

since

$$\begin{aligned} & \sum_{k=0}^{\infty} \sum_{i=1}^M \left(\frac{1}{2} + \sum_{j \neq i} \frac{w_{ij}}{\beta} \right) \|\mathcal{G}_k^{(i)} - \mathcal{G}_{k+1}^{(i)}\|_F^2 \\ & \leq \sum_{k=0}^{\infty} \left(\mathfrak{L} \left(\{\mathcal{G}_k^{(i)}\}_{i=1}^M, \{U_n^{[k]}\}_{n=1}^3 \right) - \mathfrak{L} \left(\{\mathcal{G}_{k+1}^{(i)}\}_{i=1}^M, \{U_n^{[k+1]}\}_{n=1}^3 \right) \right) \\ & \leq \mathfrak{L} \left(\{\mathcal{G}_0^{(i)}\}_{i=1}^M, \{U_n^{[0]}\}_{n=1}^3 \right) \end{aligned}$$

where the last inequality is due to the nonnegativity of the objective function \mathfrak{L} .

Moreover, if the sequence generated by Algorithm 1 converges, it will converge to a stationary point of problem (6), as stated below.

Theorem 3.3. If the sequence generated by Algorithm 1, say $\left\{ \mathcal{H}^k := \left(\{\mathcal{G}_k^{(i)}\}_{i=1}^M, \{U_n^{[k]}\}_{n=1}^3 \right) \right\}$, is convergent, i.e., there exists some \mathcal{H}^* such that $\lim_{k \rightarrow \infty} \mathcal{H}^k = \mathcal{H}^*$, then \mathcal{H}^* is a stationary point of problem (6).

4 Experimental Evaluation

In this section, numerical experiments will be implemented on the benchmark databases including the BU-3DFE database [48] and the Bosphorus database [34], and comparison results to state-of-the-art methods in this domain and other Tucker decomposition based algorithms from other applications will be reported to evaluate the effectiveness of our proposed approach (FERETMR) in facial expression recognition.

4.1 Implementation Details

4.1.1 Databases

BU-3DFE database and the Bosphorus database are two benchmark databases for FER. BU-3DFE database consists of 100 subjects (44 males and 56 females) with various ethnic backgrounds, and for each subject, there has a neutral expression and six prototypic expressions of four intensity levels,

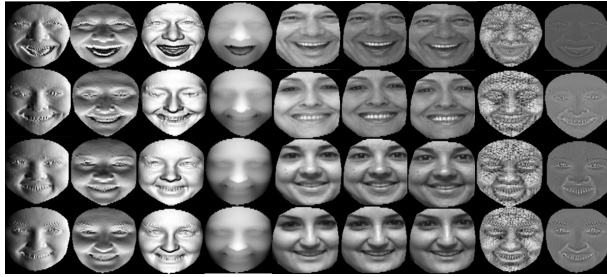


Figure 4: Illustration of different types of features of two 3D face scans with happiness expression in Bosphorus database. From top to bottom are subjects bs006, bs044, bs101 and bs104, and from left to right are Normal maps in the three directions (x, y, z), the depth maps, 3-channel 2D texture information (R, G, B), and curvature maps (curvature and mean curvature).

ranging from 1 to 4. The Bosphorus database contains 105 subjects composed of 65 males and 45 females in a variety of poses, expressions, and occlusion conditions. Unlike BU-3DFE database, only 65 subjects have six facial expressions without intensity levels in Bosphorus database.

4.1.2 Protocols

Five different protocols, termed as Setups I to V, will be used in our numerical experiments, where Setup IV is tailored for the Bosphorus database and the other four are for BU-3DFE database. More specifically, 60 out of 100 subjects with samples of the two highest intensity levels, in a given fixed order and in random, are selected in Setups I and II respectively, and all these 100 subjects are selected in Setup III, for 10-fold cross-validation. For all these three setups, 100 rounds are conducted and the average score is obtained as the final recognition accuracy. To facilitate the comparison with other existing methods, a more flexible protocol Setup V is adopted with less than 20 times to calculate the final recognition accuracy (See the details in Table 2). Since Bosphorus database only contains 65 subjects with six facial expressions, Setup IV uses the scheme in Setup II on BU-3DFE database, by replacing the total number 100 with 65.

4.1.3 Feature Selection

In the experiments, we select nine effective and discriminative features to construct the 3D tensors $\{\mathcal{X}^{(i)}\} \in \mathbb{R}^{128 \times 128 \times 9}$ after LBP descriptor [35] that is popularly applied into both 2D and 3D domain, the validation of which will be shown in Section IV(D). In BU-3DFE database, these features by 2D maps are Depth map I_g , Normal maps in three directions I_n^x, I_n^y and I_n^z , curvature maps (i.e., curvature I_c and mean curvature I_{mc}), and Textured maps in three channels I_t^r, I_t^g and I_t^b that introduced in [22,25]. Different from BU-3DFE database, the 3-channel textured features in Bosphorus database are obtained directly because the textured information of 3D face scans are provided poorly in Bosphorus database. It is worth mentioning that the 3-channel textured features in Bosphorus database are all masked by a common template to remove redundant parts. Fig. 4 shows the nine types of features of 2D maps and 2D texture information of four 3D face scans in Bosphorus database.

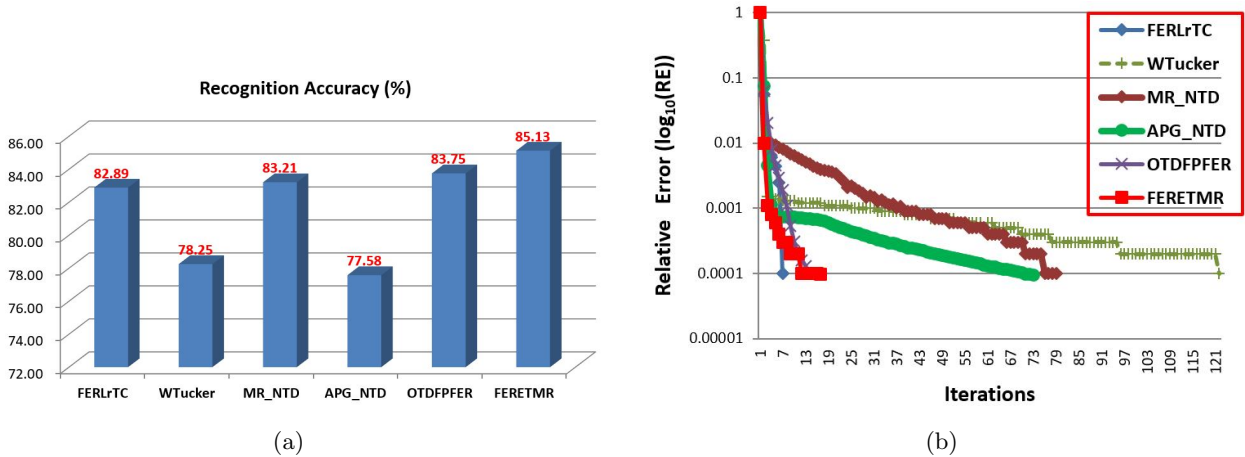


Figure 5: Comparison results of average recognition accuracies and convergence behavior on BU-3DFE database by using Setup I.

4.1.4 Parameter Setting

To better tune the parameters γ , β and k (i.e., the k -nearest neighbors), we vary the values of γ from $\{1e^i\}_{i=1}^{10}$, β from $\{1e^{-i}\}_{i=1}^{10}$ and k from $\{1, \dots, 10\}$, and find a best setting with $\gamma = 1e4$, $\beta = 1e-6$ and $k = 4$. The details about the parameter selection are shown in Section *D*.

4.1.5 Stopping Criterion

As shown in Theorem 3.2, our proposed approach generates a non-increasing sequence of objective values, which is also visualized in the red curve in Fig. 5(b). Thus, it is natural to use the relative difference between two consecutive objective values for the stopping criterion of our algorithm:

$$\frac{\left| \mathfrak{L}(\{\mathcal{G}_{k+1}^{(i)}\}_{i=1}^M, \{U_n^{[k+1]}\}_{n=1}^3) - \mathfrak{L}(\{\mathcal{G}_k^{(i)}\}_{i=1}^M, \{U_n^{[k]}\}_{n=1}^3) \right|}{\|\mathcal{X}\|_F} < \zeta$$

where $\mathcal{X} = [\mathcal{X}^{(1)}, \mathcal{X}^{(2)}, \dots, \mathcal{X}^{(M)}]$ and ζ is the accuracy parameter which is set to be $1e-4$ in our numerical experiments.

4.2 Performance Evaluation on BU-3DFE Database

Our first group of numerical experiments are implemented on BU-3DFE database. To evaluate the performance of our proposed approach, comparisons are conducted in three respects including the comparison by using our approach with Setups I, II and III as stated in Subsection A, the comparison of our approach with five other existing tensor Tucker decomposition based algorithms, and the comparison with more other state-of-the-art methods.

4.2.1 Comparison in Different Protocols

Table 1 collects the comparison results on BU-3DFE database using Setups I, II and III. As one can see, Setup I achieves the best result 85.13%, which only uses the higher intensity levels, while Setup

Table 1: Average confuse matrix on BU-3DFE database using different protocols.

%	AN	DI	FE	HA	SA	SU
AN	78.85	6.67	2.01	0.00	11.88	0.59
DI	8.66	81.25	5.52	2.61	0.00	1.96
FE	1.89	8.23	76.51	8.54	3.54	1.29
HA	0.00	1.16	2.87	95.53	0.00	0.44
SA	10.69	2.76	5.29	0.00	81.26	0.00
SU	0.17	0.33	1.58	0.56	0.00	97.36
Setup I	85.13%					
%	AN	DI	FE	HA	SA	SU
AN	79.12	6.07	4.54	0.00	9.61	0.66
DI	7.22	80.56	5.04	1.65	2.44	3.09
FE	5.21	6.44	71.49	7.34	6.21	3.31
HA	0.00	0.80	3.76	95.03	0.00	0.41
SA	13.49	3.32	5.08	0.82	77.29	0.00
SU	0.37	1.24	1.69	0.19	0.00	96.51
Setup II	83.33%					
%	AN	DI	FE	HA	SA	SU
AN	74.76	7.97	3.39	0.00	12.99	0.89
DI	10.28	77.99	4.65	1.16	3.17	2.75
FE	6.17	2.54	69.39	10.85	8.02	3.03
HA	0.40	0.86	5.62	92.93	0.00	0.19
SA	11.97	2.65	10.19	1.40	73.79	0.00
SU	0.09	3.20	2.56	0.51	0.00	93.64
Setup III	80.42%					

III obtains the worst 80.42%, which utilizes four intensity levels from 1 to 4. The comparison results indicates higher-intensity facial expressions are easier to be recognized than all-intensity expressions including lower-intensity levels (i.e., 1-level and 2-level). Among the three protocols, two expressions of happiness and surprise are achieved better recognition results because of their higher facial deformation, whereas fear expression that can be confused with other five expressions is obtained worse results and is to a great degree confused with happiness expression. Meanwhile, it can be found that sadness expression in Setup I is achieved the best recognition result among the three protocols, and even indicates a certain improvement compared with those in [16, 17, 20, 22, 25, 46].

4.2.2 Comparison with Tucker Decomposition-based Algorithms

Five state-of-the-art algorithms based on Tucker decomposition are compared with our proposed approach, which includes FERLrTC [17], WTucker [12], MR_NTD [26], APG_NTD [43] and OTDF-PFER [16].

- FERLrTC: A low-rank tensor completion approach via the nuclear-norm of factor matrices, together with the log-sum surrogate of the core tensor, is working on 4D tensor data, and a majorization minimization method is designed to solve the problem.
- MR_NTD: A manifold regularization term for the core tensors constructed in the Tucker decomposition is used to preserve geometric information in tensor data equipped with an alternating least squares manner.
- APG_NTD: A sparse nonnegative Tucker decomposition approach is carried out via an alternat-

ing proximal gradient.

- OTDFPFER: An effective approach based on orthogonal Tucker decomposition using factor priors (OTDFPFER) is proposed to recognize 2D+3D facial expression automatically.
- WTucker: A low-rank tensor completion approach based on some prescribed multilinear rank.

Among these approaches, OTDFPFER adopts the same cutting strategy as FERLrTC does. It is worth mentioning that the multilinear rank of APG_NTD should be predefined, and the multilinear rank should be over-estimated in WTucker. Different from APG_NTD, FERLrTC and OTDFPFER, our proposed approach use truncation accuracy thresholds to get R_n 's adaptively from tensor samples for dimensionality reduction, and MR_NTD also adopts the same method as our proposed method to reduce the dimension.

The comparison results in terms of the average recognition accuracy and the convergence behavior are presented in Fig. 5. Specifically, Fig. 5(a) reports the comparison result of average recognition accuracies with Setup I, and Fig. 5(b) shows the comparison results of convergence behavior using the log relative error $\log_{10}(\text{RE})$, where $\text{RE} := \|\mathcal{X}^{[k+1]} - \mathcal{X}^{[k]}\|_F / \|\mathcal{X}\|_F$ with $\mathcal{X}^{[k]} := \left[\mathcal{G}_k^{(1)} \prod_{n=1}^3 \times_n U_n^{[k]}, \dots, \mathcal{G}_k^{(M)} \prod_{n=1}^3 \times_n U_n^{[k]} \right]$ and $\mathcal{X} = [\mathcal{X}^{(1)}, \dots, \mathcal{X}^{(M)}]$. As one sees, our approach outperforms the others in terms of both two important measures. Particularly, our approach needs less iterations than those in the algorithms which use the over-estimated or the predefined rank strategies, which shows the advantage of the low-rankness that we have utilized via dimension reduction.

4.2.3 Comparison with Other Methods

Our proposed approach is also compared with the state-of-the-art methods in the literature for FER, and the comparison results are listed in Table 2, from which, one can see that our approach is quite competitive in all these four setups. Note that the stability of the performance can not be guaranteed in the literatures [36, 37, 41] that use the unstable protocol that run less than 20 times. Overall, our proposed approach FERETMR obtains the better performance for 2D+3D FER under different protocols compared with the state-of-the-art methods.

There are also the state-of-the-art methods that go beyond our proposed approach with higher recognition rates, see, e.g., Table 3. It is worth mentioning that higher complexity is required to construct the networks in [5, 25], or to get facial landmark localization in [24], comparing to our approach.

4.3 Performance Evaluation on Borphorus Database

Table 4 reports the average confusion matrix by using Setup IV. From this table, it is easily found that: i) Happy and Sadness expressions obtain the highest and lowest recognition accuracies respectively, which means Happy expression is the easiest to be recognized, while sadness one is the most difficult; ii) Expressions with recognition accuracy less than 70% include disgust, fear and sadness; iii) The confusion probability of angry expression with sadness expression is higher than others, and vice versa. At the same time, the same is true of confusion of fear expression with surprise expression.

Table 2: Performance comparison with the state-of-the-art on BU-3DFE database (T shows the running times).

Method	Data	Setup I	Setup II	Setup III	Setup V
Yurtkan et al. [50]	3D	-	-	-	88.28(8T)
Wang et al. [41]	3D	61.79	-	-	83.60(20T)
Fu et al. [13]	3D	-	-	-	85.802(10T)
Yurtkan et al. [49]	3D	-	-	-	90.8(10T)
Tang et al. [37]	3D	74.51	-	-	95.10(10T)
Soyel et al. [36]	3D	67.52	-	-	91.30(10T)
Lemaire et al. [22]	3D	76.61	-	-	-
Gong et al. [18]	3D	76.22	-	-	-
Berretti et al. [4]	3D	-	77.54	-	-
Azazi et al. [2]	3D	-	79.36	-	-
Li et al. [23]	3D	-	80.14	78.50	-
Zeng et al. [52]	3D	-	70.93	-	-
Fu et al. [15]	2D+3D	82.36	81.78	-	95.12(10T)
Zhao et al. [55]	2D+3D	-	-	-	82.30(10T)
Fu et al. [17]	2D+3D	82.89	80.91	78.96	95.28(10T)
Yang et al. [46]	3D	84.80	82.73	-	-
Jiang et al. [20]	2D+3D	83.31	80.75	74.1	-
Fu et al. [16]	2D+3D	83.75	81.63	-	95.49(10T)
ours	2D+3D	85.13	83.33	80.42	95.50(10T)

Table 3: The state-of-the-art surpassing our proposed approach on BU-3DFE database with Setups I , II and III.

Method	Data	Setup I (%)	Setup II (%)	Setup III (%)
Chen et al. [5]	3D	86.67	85.96	-
Li et al. [25]	2D+3D	86.86	-	81.04
		86.20		81.33
Li et al. [24]	2D+3D	86.32	-	80.42

Table 4: Average confuse matrix on Bosphorus database using Setup IV.

%	AN	DI	FE	HA	SA	SU
AN	75.29	6.21	4.27	0.10	10.80	3.33
DI	7.39	69.98	6.32	5.79	8.11	2.41
FE	6.87	2.98	65.12	2.36	4.37	18.30
HA	0.00	3.37	2.29	93.56	0.00	0.78
SA	15.40	13.62	5.84	0.00	63.32	1.82
SU	2.01	2.48	5.35	0.20	0.00	89.96
Setup IV	76.21%					

Compared with BU-3DFE database, Bosphorus database is very difficult to recognize facial expressions in this paper.

4.3.1 Comparison with Tucker Decomposition-based Algorithms

Like on BU-3DFE database, we use the same five algorithms based on Tucker decomposition (i.e., FERLrTC, WTucker, MR_NTD, APG_NTD and OTDFPFER) to compare with our proposed algorithm on Bosphorus database by using Setup IV.

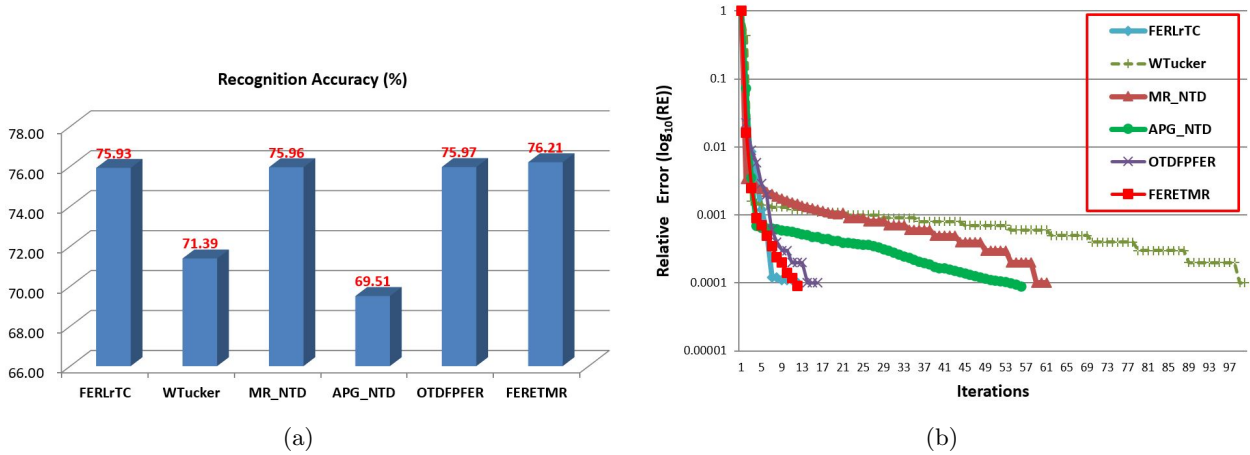


Figure 6: Comparisons of average recognition accuracies and convergence behavior on Bosphorus database using Setup IV.

The comparison results of average recognition accuracies are indicated in Fig. 6(a) by utilizing Setup IV. As can be seen from this figure, our proposed method FERETMR achieves the best performance on recognition accuracy, whereas APG_NTD obtains relatively the worst one. The comparison results in Fig. 6(a) fully illustrates that our proposed approach based on manifold regularization Tucker decomposition can extract effective features for 2D+3D facial expression. Meanwhile it is easily found that our proposed approach has a great improvement compared with the recognition accuracies of FERLrTC and OTDFPFER. These results demonstrate the Bosphorus database is very difficult to accomplish the task of 2D+3D facial expression recognition compared with BU-3DFE database. The comparison results of convergence behavior are reported in Fig. 6(b) by the relative error on Bosphorus database with Setup IV. Like on BU-3DFE database, the REs in this figure are also converge fast in limited number of iterations. The results of analysis are the same as those on BU-3DFE database.

4.3.2 Comparison with other Methods

The performance comparisons with the state-of-the-art methods (i.e., [9, 16, 17, 19, 20, 23]) are shown in Table 5 on Bosphorus database by using Setup IV. From this table, we can observe that our proposed approach obtains the highest recognition accuracy, while the method [19] gains the lowest one. Compared with the state-of-the-art methods in Table 5, our proposed approach gains better performance on Bosphorus database by using Setup IV.

4.4 Discussion

Four additional issues are discussed to further validate the effectiveness of our proposed approach (FERETMR).

Table 5: Comparison with the state-of-the-art on Bosphorus database using Setup IV.

Method	Data	Setup IV
Ujir et al. [19]	3D	63.63
Demisse et al. [9]	3D	67.05
Li et al. [23]	3D	75.83
Fu et al. [17]	2D+3D	75.93
Fu et al. [16]	2D+3D	75.97
Jiang et al. [20]	2D+3D	76.03
Ours	2D+3D	76.21

4.4.1 Parameter Selection

To better obtain the recognition accuracies of facial expression on BU-3DFE and Bosphorus databases, a best setting of the parameters R_n 's for dimensionality reduction is very important. To determine the values of R_n 's, we follow the scheme in [32]. Mathematically, for $n = 1, 2, 3$,

$$R_n = \min_{1 \leq l \leq I_n} \left\{ l : \frac{\sum_{j=1}^l \lambda_j}{\sum_{j=1}^{I_n} \lambda_j} \geq \sigma_n \right\},$$

where λ_j is the j th largest eigenvalue of $\sum_{i=1}^M X_{(n)}^{(i)} \left(X_{(n)}^{(i)} \right)^T$, and σ_n is a threshold for truncation accuracy. Four different choices of σ_n 's are used in the experiments on BU-3DFE database with Setup I, and the recognition accuracy is reported in Table 6. As shown in Table 6, the second choice $(\sigma_1, \sigma_2, \sigma_3) = (0.90, 0.90, 0.9985)$ achieves the best accuracy among all the parameter settings. Thus, we simply use this setting in all experiments on both two databases.

Table 6: Comparison on average of recognition accuracy with different threshold fitness σ in BU-3DFE database with Setup I.

	$\sigma_1 = 0.85,$ $\sigma_2=0.85,$ $\sigma_3=0.9985$	$\sigma_1=0.90,$ $\sigma_2=0.90,$ $\sigma_3=0.9985$	$\sigma_1 = 0.92,$ $\sigma_2=0.92,$ $\sigma_3=0.9985$	$\sigma_1=0.95,$ $\sigma_2=0.95,$ $\sigma_3=0.9985$
Accuracy (%)	81.75	85.13	84.28	83.90

4.4.2 Combination Effectiveness with One Feature Excluded at One Time based on Feature-Level Fusion

To verify the combination effectiveness of those nine features we have used, experiments on BU-3DFE and Bosphorus databases are conducted with one feature excluded at one time based on feature-level fusion. Table 7(a) reports the recognition accuracies and their differences with the average recognition accuracy 85.13% on BU-3DFE database by utilizing Setup I for one feature excluded at one time. From this table, we can easily observe that the difference is in the range $[-2.95, -1.01]$, among which the differences of I_n^y and I_{mc}^z achieve the lowest and highest, respectively. For Bosphorus database, the results are shown in Table 7(b). One can see that the differences with the average recognition accuracy 76.21% are in the range $[-2.20, -0.48]$, and I_g and I_{mc} obtain the lowest and

Table 7: Comparisons of recognition accuracies for one feature excluded at one time.

(a) On BU-3DFE database					
%	I_n^x	I_n^y	I_n^z	I_t^r	I_t^g
Setup I	83.01	82.18	83.23	83.09	82.98
Difference	-2.12	-2.95	-1.90	-2.04	-2.15
%	I_t^b	I_g	I_c	I_{mc}	ALL
Setup I	82.51	83.19	82.74	84.12	85.13
Difference	-2.62	-1.94	-2.39	-1.01	0.00

(b) On Bosphorus database					
%	I_n^x	I_n^y	I_n^z	I_t^r	I_t^g
Setup IV	74.25	74.12	74.52	74.22	75.07
Difference	-1.96	-2.09	-1.69	-1.99	-1.14
%	I_t^b	I_g	I_c	I_{mc}	ALL
Setup IV	74.90	74.01	74.66	75.73	76.21
Difference	-1.31	-2.20	-1.55	-0.48	0.00

Table 8: Comparisons of the recognition accuracies with different weight strategies on BU-3DFE database with Setup I.

Weight Strategy	Heat Kernel ($\delta=2$)	Heat Kernel ($\delta=1000$)	Heat Kernel ($\delta=5000$)
Accuracy(%)	84.19	84.49	84.70
Weight Strategy	Cosine	Binary	
Accuracy(%)	84.32	85.13	

highest results, respectively. The comparisons shown in Tables 7(a)-7(b) demonstrate that there exists much complementarity between 2D and 3D modalities, and validate that any of nine kinds of features can not be excluded. Therefore, it is effective to construct a set of 3D tensors by stacking nine types of features based on feature-level fusion.

4.4.3 Manifold Selection for Weight Strategy

As introduced in Section II(A), a connection between a tensor $\mathcal{X}^{(i)}$ and another tensor $\mathcal{X}^{(j)}$ has the weight w_{ij} , and the matrix W that is symmetric needs to be constructed. In this paper, we only consider the following three ways: i) the binary weight strategy in which all the elements of the matrix W are either 0 or 1; ii) the heat kernel weight scheme in which the weight value w_{ij} is achieved by $\exp(-\|\mathcal{X}^{(i)} - \mathcal{X}^{(j)}\|^2/\delta)$ where $\|\mathcal{X}^{(i)} - \mathcal{X}^{(j)}\|$ is the distance between $\mathcal{X}^{(i)}$ and $\mathcal{X}^{(j)}$. Noted that the parameter δ is difficult to be determined. We set δ to be 2, 1000, 5000, respectively; iii) the cosine weight strategy with $w_{ij} = \langle \mathcal{X}^{(i)}, \mathcal{X}^{(j)} \rangle / (\|\mathcal{X}^{(i)}\| \cdot \|\mathcal{X}^{(j)}\|)$.

Table 8 shows the comparison results with the three weight strategies on BU-3DFE database with Setup I. From this figure, it is easily observed that the binary weight scheme achieves the best result,

Table 9: Comparisons of recognition accuracy by using different feature descriptors on BU-3DFE database with Setup I.

Feature Descriptor	HOG	Dense-SIFT	Gabor	LBP
Accuracy(%)	78.87	84.05	80.51	85.13

while the heat kernel weight strategy obtains the worst one when the parameter δ is set to 2. Therefore, the binary weight strategy we use is more effective compared other schemes.

4.4.4 Feature Descriptor Selection

Since the recognition accuracy might be sensitive to the chosen local descriptor in feature extraction for accomplishing various tasks in 2D and 3D domains, we test the performances with four widely used descriptors including HOG [29], Dense-SIFT [27], Gabor [54] and LBP on BU-3DFE database with Setup I. The comparisons of recognition accuracy by using different descriptors are reported in Table 9. From this table, one can see that LBP gains the best result, while HOG obtains the worst one. Meanwhile we can observe that Dense-SIFT and LBP represent better than HOG and Gabor, and the result of LBP is higher than those of HOG, Dense-SIFT, and Gabor by 6.26%, 1.08%, and 4.62%, respectively. Therefore, we adopt the LBP descriptor since it is effective and efficient to encode local structure of textons within an image patch (See also in [47]).

5 Conclusion and Future Work

In this paper, a 2D+3D facial expression recognition approach via embedded tensor manifold regularization (FERETMR) has been proposed and solved. By employing the ℓ_1 -norm and also the tensor manifold regularization among the core tensors of samples, together with the dimension reduction scheme via truncated low-rank Tucker decomposition, we have built a nonsmooth tensor optimization problem with Stiefel manifold constraints. The first-order optimality condition via stationarity has been established, and a BCD algorithm has been designed with analysis on theoretical convergence and computation complexity. Extensive numerical experiments have been conducted on BU-3DFE database and Bosphorus database which have illustrated the effectiveness of our proposed approach.

A possible future work will be exploiting other manifold information for our constructed 3D tensors, such as the optimal Laplacian matrix introduced in [58] by considering both the local regression and global alignment. Meanwhile it is necessary to properly extract more effective features from textured 3D face scans and establish a higher-order tensor model correspondingly. The resulting tensor optimization will have a relatively large scale, and hence effective and robust algorithms are needed. All of these will be the direction of our future efforts.

6 Appendices

Proof of Theorem 3.1 It is known from [33, Theorem 10.1] that a local minimizer \mathcal{H}^* of problem (6) will satisfy $\mathcal{O} \in F(\mathcal{H}^*)$ and hence \mathcal{H}^* is a stationary point of problem (6) by Definition 1. By

employing the facts

$$\partial_{U_n} F(\mathcal{H}^*) = \nabla_{U_n} \mathfrak{L}(\mathcal{H}^*) + \partial_{U_n} \delta_{\text{St}(I_n, R_n)}(U_n)$$

and

$$\partial_{U_n} \delta_{\text{St}(I_n, R_n)}(U_n) = N_{\text{St}(I_n, R_n)}(U_n) \quad (18)$$

from [33] for $n = 1, 2, 3$, we can derive that (8) holds at \mathcal{H}^* .

Proof of Theorem 3.2 The non-increasing property of the sequence of objective values follows readily from the BCD scheme. Specifically, the update scheme as presented in (11) yields the following chain of inequalities

$$\begin{aligned} \mathfrak{L}\left(\{\mathcal{G}_k^{(i)}\}_{i=1}^M, \{U_n^{[k]}\}_{n=1}^3\right) &\geq \mathfrak{L}\left(\{\mathcal{G}_k^{(i)}\}_{i=1}^M, U_1^{[k+1]}, \{U_n^{[k]}\}_{n=2}^3\right) \\ &\geq \mathfrak{L}\left(\{\mathcal{G}_k^{(i)}\}_{i=1}^M, \{U_n^{[k+1]}\}_{n=1}^2, U_3^{[k]}\right) \\ &\geq \mathfrak{L}\left(\{\mathcal{G}_k^{(i)}\}_{i=1}^M, \{U_n^{[k+1]}\}_{n=1}^3\right) \\ &\geq \mathfrak{L}\left(\mathcal{G}_{k+1}^{(1)}, \{\mathcal{G}_k^{(i)}\}_{i=2}^M, \{U_n^{[k+1]}\}_{n=1}^3\right) \\ &\quad \vdots \\ &\geq \mathfrak{L}\left(\{\mathcal{G}_{k+1}^{(i)}\}_{i=1}^M, \{U_n^{[k+1]}\}_{n=1}^3\right). \end{aligned} \quad (19)$$

To get the desired upper bound in (17), we define

$$g_{\lambda, \alpha}(t) := \lambda|t| + \frac{\alpha}{2}(t - a)^2$$

with some $a \in \mathbb{R}$ and any given positive scalars λ and α . Denote

$$t^* := \text{Prox}_{\frac{\lambda}{\alpha}|\cdot|}(a) = \arg \min_{t \in \mathbb{R}} g_{\lambda, \alpha}(t).$$

From the optimality of t^* , we have

$$0 \in \partial g_{\lambda, \alpha, a}(t^*) = \lambda \partial |t^*| + \alpha(t^* - a),$$

i.e., there exists some $\nu \in \partial |t^*|$, such that

$$\lambda \nu + \alpha(t^* - a) = 0. \quad (20)$$

Note that $|\cdot|$ is convex, and $\nu \in \partial |t^*|$. It follows from the definition of the subdifferential of convex functions that $|t| - |t^*| \geq \nu(t - t^*), \forall t \in \mathbb{R}$. Thus,

$$\begin{aligned} &g_{\lambda, \alpha}(t) - g_{\lambda, \alpha}(t^*) \\ &= \lambda(|t| - |t^*|) + \frac{\alpha}{2}((t - a)^2 - (t^* - a)^2) \\ &\geq \lambda \nu(t - t^*) + (\alpha(t^* - a)(t - t^*) + \frac{\alpha}{2}(t - t^*)^2) \\ &= (\lambda \nu + \alpha(t^* - a))(t - t^*) + \frac{\alpha}{2}(t - t^*)^2 \\ &= \frac{\alpha}{2}(t - t^*)^2, \end{aligned} \quad (21)$$

where the last equality is from (20). Therefore,

$$\begin{aligned}
& \mathfrak{L} \left(\{\mathcal{G}_k^{(i)}\}_{i=1}^M, \{U_n^{[k+1]}\}_{n=1}^3 \right) - \mathfrak{L} \left(\mathcal{G}_{k+1}^{(1)}, \{\mathcal{G}_k^{(i)}\}_{i=2}^M, \{U_n^{[k+1]}\}_{n=1}^3 \right) \\
&= \frac{1}{\gamma} \left(\left\| \mathcal{G}_k^{(1)} \right\|_1 - \left\| \mathcal{G}_{k+1}^{(1)} \right\|_1 \right) + \frac{1}{2} \left\| \mathcal{X}^{(1)} - \mathcal{G}_k^{(1)} \prod_{n=1}^3 \times_n U_n^{[k+1]} \right\|_F^2 \\
&\quad - \frac{1}{2} \left\| \mathcal{X}^{(1)} - \mathcal{G}_{k+1}^{(1)} \prod_{n=1}^3 \times_n U_n^{[k+1]} \right\|_F^2 \\
&\quad + \frac{1}{\beta} \sum_{j=2}^M \left(\left\| \mathcal{G}_k^{(1)} - \mathcal{G}_k^{(j)} \right\|_F^2 - \left\| \mathcal{G}_{k+1}^{(1)} - \mathcal{G}_k^{(j)} \right\|_F^2 \right) w_{1j} \\
&=: \sum_{i_1, i_2, i_3} \left(g_{\frac{1}{\gamma}, a^{(1)}} \left(\left(\mathcal{G}_k^{(1)} \right)_{i_1 i_2 i_3} \right) - g_{\frac{1}{\gamma}, a^{(1)}} \left(\left(\mathcal{G}_{k+1}^{(1)} \right)_{i_1 i_2 i_3} \right) \right) \\
&\geq \frac{a^{(1)}}{2} \sum_{i_1, i_2, i_3} \left(\left(\mathcal{G}_k^{(1)} \right)_{i_1 i_2 i_3} - \left(\mathcal{G}_{k+1}^{(1)} \right)_{i_1 i_2 i_3} \right)^2 \\
&= \frac{a^{(1)}}{2} \left\| \mathcal{G}_k^{(1)} - \mathcal{G}_{k+1}^{(1)} \right\|_F^2, \tag{22}
\end{aligned}$$

where $a^{(1)} := 1 + 2 \sum_{j \neq 1}^M \frac{w_{1j}}{\beta}$, and the last inequality is from (21). Similarly, we have

$$\mathfrak{L} \left(\mathcal{G}_{k+1}^{(1)}, \{\mathcal{G}_k^{(i)}\}_{i=2}^M, \{U_n^{[k+1]}\}_{n=1}^3 \right) - \mathfrak{L} \left(\mathcal{G}_{k+1}^{(1)}, \mathcal{G}_{k+1}^{(2)}, \{\mathcal{G}_k^{(i)}\}_{i=3}^M, \{U_n^{[k+1]}\}_{n=1}^3 \right) \geq \frac{a^{(2)}}{2} \left\| \mathcal{G}_k^{(2)} - \mathcal{G}_{k+1}^{(2)} \right\|_F^2, \tag{23}$$

⋮

$$\mathfrak{L} \left(\{\mathcal{G}_{k+1}^{(i)}\}_{i=1}^{M-1}, \mathcal{G}_k^{(M)}, \{U_n^{[k+1]}\}_{n=1}^3 \right) - \mathfrak{L} \left(\{\mathcal{G}_{k+1}^{(i)}\}_{i=1}^M, \{U_n^{[k+1]}\}_{n=1}^3 \right) \geq \frac{a^{(M)}}{2} \left\| \mathcal{G}_k^{(M)} - \mathcal{G}_{k+1}^{(M)} \right\|_F^2, \tag{24}$$

with $a^{(i)} := 1 + 2 \sum_{j \neq i} \frac{w_{ij}}{\beta}$, $i = 2, \dots, M$. Consequently, for any given $k \geq 0$, we have

$$\begin{aligned}
& \mathfrak{L} \left(\{\mathcal{G}_k^{(i)}\}_{i=1}^M, \{U_n^{[k]}\}_{n=1}^3 \right) - \mathfrak{L} \left(\{\mathcal{G}_{k+1}^{(i)}\}_{i=1}^M, \{U_n^{[k+1]}\}_{n=1}^3 \right) \\
&\geq \mathfrak{L} \left(\{\mathcal{G}_k^{(i)}\}_{i=1}^M, \{U_n^{[k+1]}\}_{n=1}^3 \right) - \mathfrak{L} \left(\{\mathcal{G}_{k+1}^{(i)}\}_{i=1}^M, \{U_n^{[k+1]}\}_{n=1}^3 \right) \\
&= \mathfrak{L} \left(\{\mathcal{G}_k^{(i)}\}_{i=1}^M, \{U_n^{[k+1]}\}_{n=1}^3 \right) - \mathfrak{L} \left(\mathcal{G}_{k+1}^{(1)}, \{\mathcal{G}_k^{(i)}\}_{i=2}^M, \{U_n^{[k+1]}\}_{n=1}^3 \right) \\
&\quad + \mathfrak{L} \left(\mathcal{G}_{k+1}^{(1)}, \{\mathcal{G}_k^{(i)}\}_{i=2}^M, \{U_n^{[k+1]}\}_{n=1}^3 \right) - \mathfrak{L} \left(\mathcal{G}_{k+1}^{(1)}, \mathcal{G}_{k+1}^{(2)}, \{\mathcal{G}_k^{(i)}\}_{i=3}^M, \{U_n^{[k+1]}\}_{n=1}^3 \right) \\
&\quad \vdots \\
&\quad + \mathfrak{L} \left(\{\mathcal{G}_{k+1}^{(i)}\}_{i=1}^{M-1}, \mathcal{G}_k^{(M)}, \{U_n^{[k+1]}\}_{n=1}^3 \right) - \mathfrak{L} \left(\{\mathcal{G}_{k+1}^{(i)}\}_{i=1}^M, \{U_n^{[k+1]}\}_{n=1}^3 \right) \\
&\geq \sum_{i=1}^M \frac{a^{(i)}}{2} \left\| \mathcal{G}_k^{(i)} - \mathcal{G}_{k+1}^{(i)} \right\|_F^2 = \sum_{i=1}^M \left(\frac{1}{2} + \sum_{j \neq i} \frac{w_{ij}}{\beta} \right) \left\| \mathcal{G}_k^{(i)} - \mathcal{G}_{k+1}^{(i)} \right\|_F^2, \tag{25}
\end{aligned}$$

where the first inequality follows from (19) and the last inequality from (22) and (23).

Proof of Theorem 3.3 Several essential lemmas are proposed before proceeding the proof of Theorem 3.3.

Lemma 6.1. Let $\{A_k\} \subseteq \mathbb{R}^{m \times n}$ ($m \geq n$) be an infinite sequence and $A_k \rightarrow A_*$. Denote $B_k := U_k V_k^T$ where $U_k \in \text{St}(m, n)$ and $V_k \in \text{St}(n \times n)$ are from the SVD $A_k = U_k \Sigma_k V_k^T$. If $B_k \rightarrow B_*$, then there exist $U_* \in \text{St}(m, n)$, $V_* \in \text{St}(n \times n)$, and a diagonal matrix $\Sigma_* \in \mathbb{R}^{n \times n}$ such that $A_* = U_* \Sigma_* V_*^T$ and $B_* = U_* V_*^T$.

Proof. Since $\{V_k\}$ is bounded, there exists a convergent subsequence $V_{k_i} \rightarrow V_*$. It further yields that

$$U_{k_i} = B_{k_i} V_{k_i} \rightarrow B_* V_* =: U_*,$$

which implies that $\Sigma_{k_i} = U_{k_i}^T A_{k_i} V_{k_i} \rightarrow U_*^T A_* V_* =: \Sigma_*$. Thus, $B_{k_i} = U_{k_i} V_{k_i}^T \rightarrow U_* V_*^T = B_*$ since $B_k \rightarrow B_*$. Similarly, we have $A_{k_i} = U_{k_i} \Sigma_{k_i} V_{k_i}^T \rightarrow U_* \Sigma_* V_*^T = A_*$, since $A_k \rightarrow A_*$. This completes the proof.

By employing the optimality theorem for constrained nonlinear programming, we have the following lemma.

Lemma 6.2. Given $X_1, \dots, X_M \in \mathbb{R}^{m \times q}$, $\Phi_1, \dots, \Phi_M \in \mathbb{R}^{n \times q}$, $U_* \in \mathbb{R}^{m \times n}$ ($q \geq m \geq n$), let $A_* := \sum_{i=1}^M X_i \Phi_i^T$. If $U_* = \text{qf}(A_*)$, then

$$O \in \nabla \left(\frac{1}{2} \sum_{i=1}^M \|X_i - U_* \Phi_i\|_F^2 \right) + N_{\text{St}(m, n)}(U_*).$$

Proof. Since $U_* = \text{qf}(A_*)$, we have

$$\begin{aligned} U_* &= \arg \max_{U \in \text{St}(m, n)} \langle A_*, U \rangle \\ &= \arg \min_{U \in \text{St}(m, n)} \frac{1}{2} \sum_{i=1}^M \|X_i - U \Phi_i\|_F^2 \\ &= \arg \min_{U \in \mathbb{R}^{m \times n}} \left\{ \frac{1}{2} \sum_{i=1}^M \|X_i - U \Phi_i\|_F^2 + \delta_{\text{St}(m, n)}(U) \right\} \end{aligned}$$

By invoking [33, Theorem 10.1], we have

$$O \in \partial \left(\frac{1}{2} \sum_{i=1}^M \|X_i - U_* \Phi_i\|_F^2 + \delta_{\text{St}(m, n)}(U_*) \right).$$

Note that the function $\frac{1}{2} \sum_{i=1}^M \|X_i - U \Phi_i\|_F^2$ is continuously differentiable in U . Combining with (18), we have

$$\begin{aligned} &\partial \left(\frac{1}{2} \sum_{i=1}^M \|X_i - U_* \Phi_i\|_F^2 + \delta_{\text{St}(m, n)}(U_*) \right) \\ &= \nabla \left(\frac{1}{2} \sum_{i=1}^M \|X_i - U_* \Phi_i\|_F^2 \right) + N_{\text{St}(m, n)}(U_*). \end{aligned}$$

This completes the proof of the lemma.

By utilizing the first-order optimality theorem for convex programming, we also have the following equivalence.

Lemma 6.3. Given $\mathcal{G}^*, \mathcal{W}^* \in \mathbb{R}^{R_1 \times R_2 \times R_3}$, and $\tau > 0$, then $\mathcal{G}^* = \text{Prox}_{\tau \|\cdot\|_1}(\mathcal{W}^*)$ if and only if

$$\mathcal{O} \in \partial(\tau \|\mathcal{G}^*\|_1) + \mathcal{G}^* - \mathcal{W}^*.$$

Now we are in a position to prove Theorem 3.3. According to the update scheme as presented in (11), together with the closed-form solutions established in (12) and (16), we have

$$\left\{ \begin{array}{l} U_1^{[k+1]} = \text{qf} \left(\sum_{i=1}^M X_{(1)}^{(i)} \left(\mathcal{G}_k^{(i)} \times_2 U_2^{[k]} \times_3 U_3^{[k]} \right)_{(1)} \right), \\ U_2^{[k+1]} = \text{qf} \left(\sum_{i=1}^M X_{(2)}^{(i)} \left(\mathcal{G}_k^{(i)} \times_1 U_1^{[k+1]} \times_3 U_3^{[k]} \right)_{(2)} \right), \\ U_3^{[k+1]} = \text{qf} \left(\sum_{i=1}^M X_{(3)}^{(i)} \left(\mathcal{G}_k^{(i)} \times_1 U_1^{[k+1]} \times_2 U_2^{[k+1]} \right)_{(3)} \right), \\ \mathcal{G}_{k+1}^{(1)} = \text{Prox}_{\tau^{(1)} \|\cdot\|_1} \left(\frac{\beta \mathcal{X}^{(1)} \Pi_{n=1}^3 \times_n (U_n^{[k+1]})^T + \sum_{j \neq 1} w_{1j} \mathcal{G}_k^{(j)}}{\beta + 2 \sum_{j \neq 1} w_{1j}} \right), \\ \vdots \\ \mathcal{G}_{k+1}^{(M)} = \text{Prox}_{\tau^{(M)} \|\cdot\|_1} \left(\frac{\beta \mathcal{X}^{(M)} \Pi_{n=1}^3 \times_n (U_n^{[k+1]})^T + \sum_{j \neq M} w_{Mj} \mathcal{G}_k^{(j)}}{\beta + 2 \sum_{j \neq M} w_{Mj}} \right), \end{array} \right. \quad (26)$$

From the hypothesis, we have

$$\left\{ \begin{array}{l} \lim_{k \rightarrow \infty} \mathcal{G}_k^{(i)} = (\mathcal{G}^{(i)})^*, \quad i = 1, \dots, M, \\ \lim_{k \rightarrow \infty} U_n^{[k]} = U_n^*, \quad n = 1, 2, 3. \end{array} \right. \quad (27)$$

Taking limit $k \rightarrow \infty$ on both sides of all equations in (26), it then follows from Lemma 6.1 and the continuity of $\text{Prox}_{\tau^{(i)} \|\cdot\|_1}(\cdot)$ (See, Fig. 3) that

$$\left\{ \begin{array}{l} U_1^* = \text{qf} \left(\sum_{i=1}^M X_{(1)}^{(i)} \left((\mathcal{G}^{(i)})^* \times_2 U_2^* \times_3 U_3^* \right)_{(1)} \right), \\ U_2^* = \text{qf} \left(\sum_{i=1}^M X_{(2)}^{(i)} \left((\mathcal{G}^{(i)})^* \times_1 U_1^* \times_3 U_3^* \right)_{(2)} \right), \\ U_3^* = \text{qf} \left(\sum_{i=1}^M X_{(3)}^{(i)} \left((\mathcal{G}^{(i)})^* \times_1 U_1^* \times_2 U_2^* \right)_{(3)} \right), \\ (\mathcal{G}^{(1)})^* = \text{Prox}_{\tau^{(1)} \|\cdot\|_1} \left(\frac{\beta \mathcal{X}^{(1)} \Pi_{n=1}^3 \times_n U_n^* + \sum_{j \neq 1} w_{1j} (\mathcal{G}^{(j)})^*}{\beta + 2 \sum_{j \neq 1} w_{1j}} \right), \\ \vdots \\ (\mathcal{G}^{(M)})^* = \text{Prox}_{\tau^{(M)} \|\cdot\|_1} \left(\frac{\beta \mathcal{X}^{(M)} \Pi_{n=1}^3 \times_n U_n^* + \sum_{j \neq M} w_{Mj} (\mathcal{G}^{(j)})^*}{\beta + 2 \sum_{j \neq M} w_{Mj}} \right), \end{array} \right. \quad (28)$$

In virtue of Lemmas 6.2 and 6.3, we can conclude that $\mathcal{H}^* = \left(\{(\mathcal{G}^{(i)})^*\}_{i=1}^M, \{U_n^*\}_{n=1}^3 \right)$ satisfies (8) and hence \mathcal{H}^* is a stationary point of problem (6).

Acknowledgment

The authors sincerely appreciated the editor and anonymous referees for their valuable comments and suggestions. This work was partly supported by the National Natural Science Foundation of China (61471032, 11771038, 61772067), the fundamental research funds for the central universities (2017JBZ108), Beijing Natural Science Foundation (Z190002), Innovation Capability Improvement Plan Project of Hebei Science and Technology Department(21557611K), and Hebei Province Internet of Things Intelligent Perception and Application Technology Innovation Center.

References

- [1] Jinliang An, Xiangrong Zhang, Huiyu Zhou, and Licheng Jiao. Tensor-based low-rank graph with multimanifold regularization for dimensionality reduction of hyperspectral images. *IEEE Trans. Geosci. Remote Sensing*, PP(99):1–16, 2018.
- [2] Amal Azazi, Syaheerah Lebai Lutfi, and Ibrahim Venkat. Analysis and evaluation of surf descriptors for automatic 3D facial expression recognition using different classifiers. In *Inf. Commun. Technol.*, pages 23–28, 2014.
- [3] Amir Beck and Marc Teboulle. A fast iterative shrinkage-thresholding algorithm for linear inverse problems. *SIAM J. Imaging Sci.*, 2(1):183–202, 2009.
- [4] Stefano Berretti, Alberto Del Bimbo, Pietro Pala, Boulbaba Ben Amor, and Mohamed Daoudi. A set of selected sift features for 3D facial expression recognition. In *Proc. Int. Conf. Pattern Recog.*, pages 4125–4128, 2010.
- [5] Zhixing Chen, Di Huang, Yunhong Wang, and Liming Chen. Fast and light manifold cnn based 3D facial expression recognition across pose variations. In *ACM Multimedia Conf. Multimedia Conf.*, pages 229–238. ACM, 2018.
- [6] Hong Cheng. Sparse representation, modeling and learning in visual recognition: Theory, algorithms and applications. *Adv. Comput. Vis. Pattern Recog.*, 93(6):1408–1425, 2015.
- [7] C. A. Corneanu, M. Oliu, J. F. Cohn, and S. Escalera. Survey on rgb, 3D, thermal, and multimodal approaches for facial expression recognition: History, trends, and affect-related applications. *IEEE Trans. Pattern Anal. Mach. Intell.* , 38(8):1548–1568, 2016.
- [8] Mohamed Dahmane and Jean Meunier. Prototype-based modeling for facial expression analysis. *IEEE Trans. Multimedia*, 16(6):1574–1584, 2014.
- [9] Girum G. Demisse, Djamila Aouada, and Bjorn Ottersten. Deformation based 3D facial expression representation. *ACM Trans. Multimedia Comput. Commun. Appl.*, 14(1s), 2018.
- [10] D. L. Donoho. Compressed sensing. *IEEE Trans. Inform. Theory.* , 52(4):1289–1306, 2006.
- [11] Alan Edelman, Tomas A Arias, and Steven T Smith. The geometry of algorithms with orthogonality constraints. *SIAM J. Matrix Anal. Appl.*, 20(2):303–353, 1998.
- [12] Marko Filipović and Ante Jukić. Tucker factorization with missing data with application to low-rank tensor completion. *Multidimens. Syst. Signal Process.*, 26(3):1–16, 2015.
- [13] Yunfang Fu, Qiuqi Ruan, Gaoyun An, and Yi Jin. Fast nonnegative tensor factorization based on graph-preserving for 3D facial expression recognition. In *IEEE Int. Conf. Signal Process.* , pages 292–297, 2017.
- [14] Yunfang Fu, Qiuqi Ruan, and Yiajie Jiang. Sparse and low-rank tucker decomposition with its application to 2D+3D facial expression recognition. In *IEEE Int. Conf. Signal Process.* , pages 37–44, 2020.

- [15] Yunfang Fu, Qiuqi Ruan, Yi Jin, and Gaoyun An. Sparse orthogonal tucker decomposition for 2D+3D facial expression recognition. In *IEEE Int. Conf. Signal Process.*, pages 516–521, 2018.
- [16] Yunfang Fu, Qiuqi Ruan, Luo Ziyang, Gaoyun An, and Yi Jin. Orthogonal tucker decomposition using factor priors for 2D+3D facial expression recognition. *IET Biometrics.*, 10:664–678, 2021.
- [17] Yunfang Fu, Qiuqi Ruan, Luo Ziyang, Yi Jin, Gaoyun An, and Wan Jun. FERLrTC: 2D+3D facial expression recognition via low-rank tensor completion. *Signal Process.*, 161(4):74–88, 2019.
- [18] Boqing Gong, Yueming Wang, Jianzhuang Liu, and Xiaoou Tang. Automatic facial expression recognition on a single 3D face by exploring shape deformation. In *Proc. ACM Int. Conf. Multimedia* , pages 569–572, 2009.
- [19] Ujir Hamimah and Michael Spann. Surface normals with modular approach and weighted voting scheme in 3D facial expression classification. *Int. J. Comput. Inf. Technol.* , 3(05), 2014.
- [20] Yiajie Jiang and Qiuqi Ruan. Multi-feature tensor neighborhood preserving embedding for 3D facial expression recognition. *IEEE Access*, 9:106303–106316, 2021.
- [21] Yiajie Jiang, Qiuqi Ruan, and Yunfang Fu. Sparse multi-feature tensor representation for 3D facial expression recognition. In *IEEE Int. Conf. Signal Process.* , pages 300–305, 2020.
- [22] Pierre Lemaire, Mohsen Ardabilian, Liming Chen, and Mohamed Daoudi. Fully automatic 3D facial expression recognition using differential mean curvature maps and histograms of oriented gradients. In *Proc. IEEE Int. Conf. Workshops Automat. Face Gesture Recog.* , pages 1–7, 2013.
- [23] Huibin Li, Liming Chen, Di Huang, and Yunhong Wang. 3D facial expression recognition via multiple kernel learning of multi-scale local normal patterns. In *Int. Conf. Pattern Recog.*, pages 2577–2580, 2012.
- [24] Huibin Li, Huaxiong Ding, Di Huang, Yunhong Wang, Xi Zhao, Jean Marie Morvan, and Liming Chen. An efficient multimodal 2D + 3D feature-based approach to automatic facial expression recognition. *Comput. Vis. Image Underst.*, 140(SCIA):83–92, 2015.
- [25] Huibin Li, Jian Sun, Zongben Xu, and Liming Chen. Multimodal 2D+3D facial expression recognition with deep fusion convolutional neural network. *IEEE Trans. Multimedia*, 19(12):2816–2831, 2017.
- [26] X. Li, M. K. Ng, G. Cong, Y. Ye, and Q. Wu. MR-NTD: Manifold regularization nonnegative tucker decomposition for tensor data dimension reduction and representation. *IEEE Trans. Neural Netw. Learn. Syst.*, 28(8):1787, 2017.
- [27] Ce Liu, Jenny Yuen, and Antonio Torralba. Sift flow: Dense correspondence across scenes and its applications. *IEEE Trans. Pattern Anal. Mach. Intell.*, 33(5):978–994, 2011.
- [28] L. Mirsky. A trace inequality of john von neumann. *Monats. Math.*, 79(4):303–306, 1975.

- [29] Dalal Navneet and Triggs Bill. Histograms of oriented gradients for human detection. In *IEEE Soc. Conf. Comput. Vis. Pattern Recog.*, pages 886–893, 2005.
- [30] Maja Pantic and Leon J. M Rothkrantz. Automatic analysis of facial expressions: The state of the art. *IEEE Trans. Pattern Anal. Mach. Intell.*, 22(12):1424–1445, 2000.
- [31] V. Perez-Gomez, H. V. Rios-Figueroa, E. J. Rechy-Ramirez, E. Mezura-Montes, and A. Marin-Hernandez. Feature selection on 2D and 3D geometric features to improve facial expression recognition. *Sensors*, 20:4847–4866, 2020.
- [32] Anh Huy Phan and Andrzej Cichocki. Tensor decompositions for feature extraction and classification of high dimensional datasets. *Nonlinear Theory Appl. Ieice*, 1(1):37–68, 2010.
- [33] R. Tyrrell Rockafellar and Roger J. B Wets. *Variational Analysis*. Springer, 2013.
- [34] Arman Savran, Neşe Alyüz, Hamdi Dibeklioglu, Oya Çeliktutan, Berk Gökberk, Bülent Sankur, and Lale Akarun. Bosphorus database for 3D face analysis. In *Biometrics Identity Manag.*, pages 47–56, 2008.
- [35] Caifeng Shan, Shaogang Gong, and Peter W. Mcowan. Facial expression recognition based on local binary patterns: A comprehensive study. *Image Vis. Comput.*, 27(6):803–816, 2009.
- [36] Hamit Soyel and Hasan Demirel. Facial expression recognition using 3D facial feature distances. In *Int. Conf. Image Anal. Recog.*, pages 831–838, 2007.
- [37] Hao Tang and T. S Huang. 3D facial expression recognition based on properties of line segments connecting facial feature points. In *IEEE Int. Conf. Automat. Face Gesture Recog.*, pages 1–6, 2008.
- [38] Kun Tian, Liaoyuan Zeng, Sean McGrath, Qian Yin, and Wenyi Wang. 3D facial expression recognition using deep feature fusion CNN. *Irish Signals Syst. Conf.*, pages 1–6, 2019.
- [39] P. Tseng. Convergence of a block coordinate descent method for nondifferentiable minimization. *J. Opti. Theory Appl.*, 109(3):475–494, 2001.
- [40] Jun Wang and Lijun Yin. Static topographic modeling for facial expression recognition and analysis. *Comput. Vis. Image Underst.*, 108(1):19–34, 2005.
- [41] Jun Wang, Lijun Yin, Xiaozhou Wei, and Yi Sun. 3D facial expression recognition based on primitive surface feature distribution. In *Proc. IEEE Conf. Comput. Vis. Pattern Recog.*, volume 2, pages 1399–1406, 2006.
- [42] John Wright, Yi Ma, Julien Mairal, Guillermo Sapiro, Thomas S Huang, and Shuicheng Yan. Sparse representation for computer vision and pattern recognition. *Proc. IEEE*, 98(6):1031–1044, 2010.
- [43] Yangyang Xu. Alternating proximal gradient method for sparse nonnegative tucker decomposition. *Math. Program. Comput.*, 7(1):39–70, 2015.

- [44] Yong Xu, David Zhang, Jian Yang, and Jing Yu Yang. A two-phase test sample sparse representation method for use with face recognition. *IEEE Trans. Circuits. Syst. Video Technol.*, 21(9):1255–1262, 2011.
- [45] Jiang Yajie and Ruan Qiuqi. Low-dimensional multi-modality representation for 3D data. In *IEEE Int. Conf. Wireless, Mobile. Multimedia Netw. IET.*, pages 527–532, 2019.
- [46] Xudong Yang, Di Huang, Yunhong Wang, and Liming Chen. Automatic 3D facial expression recognition using geometric scattering representation. In *IEEE Int. Conf. Workshops Automat. Face Gesture Recog.*, pages 1–6, 2015.
- [47] Yongqiang Yao, Di Huang, Xudong Yang, Yunhong Wang, and Liming Chen. Texture and geometry scattering representation-based facial expression recognition in 2D+3D videos. *ACM Trans. Multimedia Comput. Commun. Appl.*, 14(1s):18:1–18:23, 2018.
- [48] Lijun Yin, Xiaozhou Wei, Yi Sun, Jun Wang, and Matthew J. Rosato. A 3D facial expression database for facial behavior research. In *Int. Conf. Automat. Face Gesture Recog.*, pages 211–216, 2006.
- [49] Kamil Yurtkan and Hasan Demirel. Entropy-based feature selection for improved 3D facial expression recognition. *Signal Image Video Process.*, 8(2):267–277, 2014.
- [50] Kamil Yurtkan and Hasan Demirel. Feature selection for improved 3D facial expression recognition. *Pattern Recog. Lett.*, 38(1):26–33, 2014.
- [51] Lukasz Zalewski and Shaogang Gong. Synthesis and recognition of facial expressions in virtual 3D views. In *IEEE Int. Conf. Automat. Face Gesture Recog.*, pages 493–498, 2004.
- [52] Wei Zeng, Huibin Li, Liming Chen, Jean Marie Morvan, and Xianfeng David Gu. An automatic 3D expression recognition framework based on sparse representation of conformal images. In *IEEE Int. Conf. Workshops Automat. Face Gesture Recog.*, pages 1–8, 2013.
- [53] Zheng Zhang, Yong Xu, Jian Yang, Xuelong Li, and David Zhang. A survey of sparse representation: algorithms and applications. *IEEE Access*, 3:490–530, 2017.
- [54] Zhengyou Zhang, M. Lyons, M. Schuster, and S. Akamatsu. Comparison between geometry-based and gabor-wavelets-based facial expression recognition using multi-layer perceptron. In *IEEE Int. Conf. Automat. Face Gesture Recog.*, 1998.
- [55] Xi Zhao, Di Huang, Emmanuel Dellandréa, and Liming Chen. Automatic 3D facial expression recognition based on a bayesian belief net and a statistical facial feature model. In *Int. Conf. Pattern Recog.*, pages 3724–3727, 2010.
- [56] Qingkai Zhen, Di Huang, Yunhong Wang, and Liming Chen. Muscular movement model-based automatic 3D/ 4D facial expression recognition. *IEEE Trans. Multimedia*, 18(7):1438–1450, 2016.
- [57] G. Zhong and M Cheriet. Large margin low rank tensor analysis. *Neural Comput.*, 26(4):761–780, 2014.

- [58] Yueting Zhuang, Jiebo Luo, Yi Yang, Feiping Nie, Dong Xu, and Yunhe Pan. A multimedia retrieval framework based on semi-supervised ranking and relevance feedback. *IEEE Trans. Pattern Anal. Mach. Intell.*, 34(4):723–742, 2012.